Continental Shelf Research ▮ (▮▮▮▮) ▮▮▮–▮▮▮

Contents lists available at SciVerse ScienceDirect

Continental Shelf Research

journal homepage: www.elsevier.com/locate/csr

Research papers

# Processes controlling stratification on the northern Skagit Bay tidal flats

V. Pavel *, B. Raubenheimer, Steve Elgar

*Applied Ocean Physics and Engineering, Woods Hole Oceanographic Institution, Woods Hole, MA 02543, USA*

ARTICLE INFO

*Article history:*
Received 5 December 2011
Received in revised form
21 June 2012
Accepted 26 June 2012

*Keywords:*
Skagit Bay
Intertidal flats
Stratification
Potential energy anomaly
Tidal straining

ABSTRACT

Estuarine systems range from highly stratified to well mixed, often passing through several states during a single tidal cycle. Here, the processes driving temporal and spatial variations of stratification are investigated on the broad, shallow, periodically inundated tidal flats (shoals) between the north and south forks of the Skagit River. Over a two-week period, observation-based estimates of the straining, advection, and mixing are in balance with the temporal changes in the stratification-induced potential energy anomaly at a mid-flat location. The water on the tidal flats does not completely de-stratify during the strong ebb, and thus the initial tongue of water crossing the flats on strong floods often is partly stratified, but becomes increasingly well mixed as the flood progresses. For nearly semi-diurnal tides, the maximum stratification occurs during mid-ebb tide. Although cross- and alongshore flows have similar magnitudes, the changes in stratification during semi-diurnal tides result primarily from cross-shore processes, similar to observations of narrow, strongly-forced salt-wedge estuaries. Stratification is stronger during tides with a large diurnal inequality (the elevations of the two daily low tides differ by more than 33% of the tidal range) than during nearly semi-diurnal tides (with low tide elevations that differ by less than 25% of the tidal range), and is a maximum in the middle of the weak flood that follows the small low. In contrast to prior observations in narrow estuaries, alongshore (roughly parallel to isopycnals) advection of stratified water is significant and contributes to the increased stratification during these tides. Furthermore, during the small low and weak flood, the strongly sheared (density-driven) flows, which are offshore-directed at the surface and onshore-directed at the bed, also contribute to the high levels of stratification. Temporal changes in stratification are similar across and along the flats. However, maximum stratification increases offshore and alongshore towards the north fork (the distributary channel closest to the instruments).



## 1. Introduction

Although tidal flats form a relatively small portion of the total coastal and estuarine area, they can affect the circulation patterns throughout larger basins by increasing heating rates (Kim et al., 2010; Kim and Cho, 2011), bed friction (Nicolle and Karpytchev, 2007), and tidal volume storage (Friedrichs and Aubrey, 1988), and by altering basin resonance characteristics (Fortunato et al., 1997, 1999) and nonlinear tidal interactions (Speer and Aubrey, 1985; Fortunato et al., 1999; Blanton et al., 2002). Tidal flats also can provide a coastal buffer (Kirby, 2000; Kim, 2003) and important habitat for fish and game (Grossman et al., 2007). Understanding the complicated circulation and salinity characteristics resulting from the shallow depths, periodic inundation, tidal flows, and river discharge is vital to managing these natural resources.

Intra- and intertidal variations of stratification in estuaries and on estuarine tidal flats have been shown to change circulation patterns (Monismith et al., 1996; Stacey et al., 2001; Ralston and Stacey, 2005a; Cheng et al., 2009; Becker et al., 2009), suppress turbulence (Nepf and Geyer, 1996; Peters and Bokhorst, 2001; Rippeth et al., 2001; Ralston and Stacey, 2005b; Stacey et al., 1999; Ralston et al., 2010b; Wang et al., 2011), and reduce bottom stress and suspended-sediment concentration (Chant and Stoner, 2001; Ralston and Stacey, 2007; Chen et al., 2010). The potential energy anomaly (Simpson and Bowers, 1981) often is used to quantify changes in stratification (Simpson et al., 1990; Wiles et al., 2006; Marques et al., 2010, 2011; Ralston et al., 2010). In many estuaries the potential energy anomaly owing to longitudinal tidal straining (the vertically sheared velocity profile acting on the along-channel horizontal density gradient) increases stratification and suppresses turbulent mixing on the ebb and decreases stratification and enhances mixing on the flood (Simpson et al., 1990; Chant and Stoner, 2001; Burchard and Hofmeister, 2008). In shallow salt-wedge estuaries longitudinal advection may enhance straining effects on the flood and may oppose the straining-induced increase in stratification on the ebb (Giddings et al. 2011). Vertical advection processes also may be important in regions with large, spatially inhomogeneous

* Corresponding author. Tel.: +1 626 644 1455.
*E-mail address:* vera.pavel@gmail.com (V. Pavel).

0278-4343/$ - see front matter © 2012 Elsevier Ltd. All rights reserved.
http://dx.doi.org/10.1016/j.csr.2012.06.012

horizontal density gradients (Nepf and Geyer, 1996; Burchard and Hofmeister, 2008; de Boer et al., 2008; Marques et al., 2011), whereas in estuaries with complex bathymetry and in coastal regions near river plumes (e.g., regions of freshwater influence or ROFIs) both cross- and alongshore processes contribute to the stratification (Lacy et al., 2003; de Boer et al., 2008; Marques et al., 2010). Furthermore, nonlinear effects may be important near deltaic distributary channels and estuarine inlets (de Boer et al., 2008; Marques et al., 2010), and wind-driven currents can affect the potential-energy-anomaly balance in estuaries and ROFIs during storms (Yang and Khangaonkar, 2009; Marques et al., 2010, 2011). Overall, the magnitudes of the river discharge, tidal and wind-driven currents, and horizontal density gradients influence which processes dominate the stratification balance (Nepf and Geyer, 1996; Burchard and Hofmeister, 2008; de Boer et al., 2008; Hofmeister et al., 2009). These forcing mechanisms, and thus the stratification, can vary on seasonal (Marques et al., 2010), spring-neap (Peters, 1997), storm (Marques et al., 2010, 2011), and tidal timescales (Simpson et al., 1990; Nepf and Geyer, 1996; Stacey et al., 1999; Rippeth et al., 2001).

Similar to tidal salt-wedge estuaries on the Merrimack (Ralston et al., 2010a,b), Columbia (Jay and Smith, 1990), Fraser (Geyer and Farmer, 1989), and Snohomish Rivers (Wang et al., 2009; Giddings et al., 2011), tidal flats and the associated channels are short, have strong cross-shore density gradients, and periodically are strongly stratified. Tidal-flat channels can be similar to narrow estuaries, especially during periods of high river runoff. For example, stratification that increased on ebbs and decreased on floods in a San Francisco Bay tidal-flat channel during the spring freshet was primarily a result of straining of the longitudinal density gradient and advection of the salinity front (Ralston and Stacey, 2005a,b, 2007). Just as stratification can be different in the thalweg than over the shoals of estuaries (Cheng et al., 2009), stratification on the shoals of estuarine tidal-flat regions, which make up the majority of the total surface area, can differ significantly from that in the river channels. In some cases, the water over the shoals may remain well mixed and saline, despite a stratifying freshwater influence in the channels (Ralston and Stacey, 2005b). Stratification in or near channels can result from density gradients between fast-flowing water in the channel and slower-flowing water on the shoal (Ralston and Stacey, 2005a). On tidal flats, the tidal range is greater than the mean water depth, and thus the effects of depth changes can be significant (Ralston and Stacey, 2005b, 2007; Giddings et al., 2011), and the effects of the periodic inundation and drying of tidal flats is uncertain.

Here, field observations collected for two weeks on the tidal flats (the shoals) between the north and south forks of the Skagit River (Fig. 1) are used to examine intratidal and fortnightly variations of the potential-energy-anomaly balance and to determine the relative importance of different processes to the stratification. In contrast to the flows in and near a distributary channel on the south flats (Ralston et al., in this issue), the alongshore flows (roughly parallel to bathymetry and density contours) over the flats (shoals) between the distributary channels here are similar in magnitude to the cross-shore flows. It is shown that, similar to ROFIs and to short, wide estuaries, lateral processes can be significant, with stratification modified by straining and advection of water along the flat.

## 2. Field study

### 2.1. Geographic setting

The Skagit Bay tidal flats, near La Conner, WA, have an area of about 100 km$^2$ (Fig. 1). A deep channel runs along the edge of Whidbey Island, which forms the western border of Skagit Bay. To the north and south, Skagit Bay connects with the Strait of Juan de Fuca and the rest of Puget Sound via Deception Pass and Saratoga Passage, respectively. Tides propagate northwestward from Saratoga Passage towards Deception Pass.

In contrast with many intertidal flats in low-energy environments (Banas et al., 2004; Lee et al., 2004; Fan et al., 2006), the sediment on the Skagit flats is primarily sandy (Webster et al., submitted for publication). The cross-shore bed slope is approximately 1/1000 in the study area. The spring tidal range is about 4 m, and even the lowest part of the flats are dry at lower low tide. Thus, the tidal range is larger than the mean water depth, in contrast to deeper estuaries (Nepf and Geyer, 1996; Burchard and Hofmeister, 2008) and ROFIs (de Boer et al., 2008). Tides are mixed (Fig. 2), and can be nearly semidiurnal (type 1) or nearly diurnal (type 2).

About 5 km upstream of the flats, the Skagit River splits into north and south forks that carry approximately 60% and 40% of the flow, respectively (Grossman et al., 2007; Yang and Khangaonkar, 2009). River discharge, measured at Mt. Vernon (upstream of the fork) was about 200 m$^3$/s during the study period (USGS gage 12200500 http://waterdata.usgs.gov/nwis/nwisman/?site_no=12200500). Numerous small channels (depth O(0.10–0.25 m)) split off from the north fork of the Skagit and extend across the marshes onto the tidal flats near the measurement locations (Elgar and Raubenheimer, 2011; Webster et al., submitted for publication). However, the majority of the discharge from the north and south forks exits onto the flats about 2.5 km northwest and 4.5 km southeast, respectively, of the study area.

### 2.2. Measurements

Measurements of water level, currents, and water density were collected between 18 and 31 August 2009 at 5 locations perpendicular to and along (northwest to southeast) the 0-m bathymetry contour (about 3-m maximum water depth) on the tidal flats (symbols in Fig. 1). Water density was estimated from measurements with induction-type conductivity-temperature-depth (CTD) sensors. Nearbed density was measured with a fixed CT sensor located 0.4 m above the bed (Fig. 3). Near-surface density was measured with CT and CTD sensors mounted on a pole at distances of 0.2 and 0.7 m below a surface float, respectively. The tilt of the pole, and thus the depth of the upper CT sensor, was estimated from the along-pole distances and the depth measured by the lower CTD sensor. Laboratory tests showed that errors in temperature and salinity are $<0.1$ °C and 0.1 PSU, respectively. The depth accuracy is about $\pm 0.01$ m and the density accuracy is about $\pm 0.1$ kg/m$^3$. Bottom pressure was measured at 4 Hz with pressure sensors buried $\sim$0.1 m below the bed level. Atmospheric pressure was measured at 4 Hz near La Conner, WA. Nearbed flows were measured $\sim$0.1 m above the bed with acoustic Doppler velocimeters (ADVs) (accuracy about $\pm 0.01$ m/s) that collected 3072 s of data at 2 Hz starting at the beginning of each hour. Flow profiles were measured at $\sim$2 Hz in 0.25-m bins from $\sim$0.4 m above the bed to the water surface with upward-facing 2.0-MHz acoustic Doppler current profilers (accuracy about $\pm 0.03$ m/s for 1-min averages). Instrument locations were surveyed with post-processed differential GPS (accuracy about 0.03 m). Instruments were separated in the cross- and alongshore by $\sim$600 and 1600 m, respectively. Simulations with an FVCOM model (Ralston et al., in this issue) suggest alongshore spatial scales are longer than cross-shore scales (not shown).

Density measurements were averaged over 512-s periods. At the central location, the upper floating CT failed, and the data were replaced by an average of the 4 other upper CTs. Root-mean-square

Please cite this article as: Pavel, V., et al., Processes controlling stratification on the northern Skagit Bay tidal flats. Continental Shelf Research (2012), http://dx.doi.org/10.1016/j.csr.2012.06.012

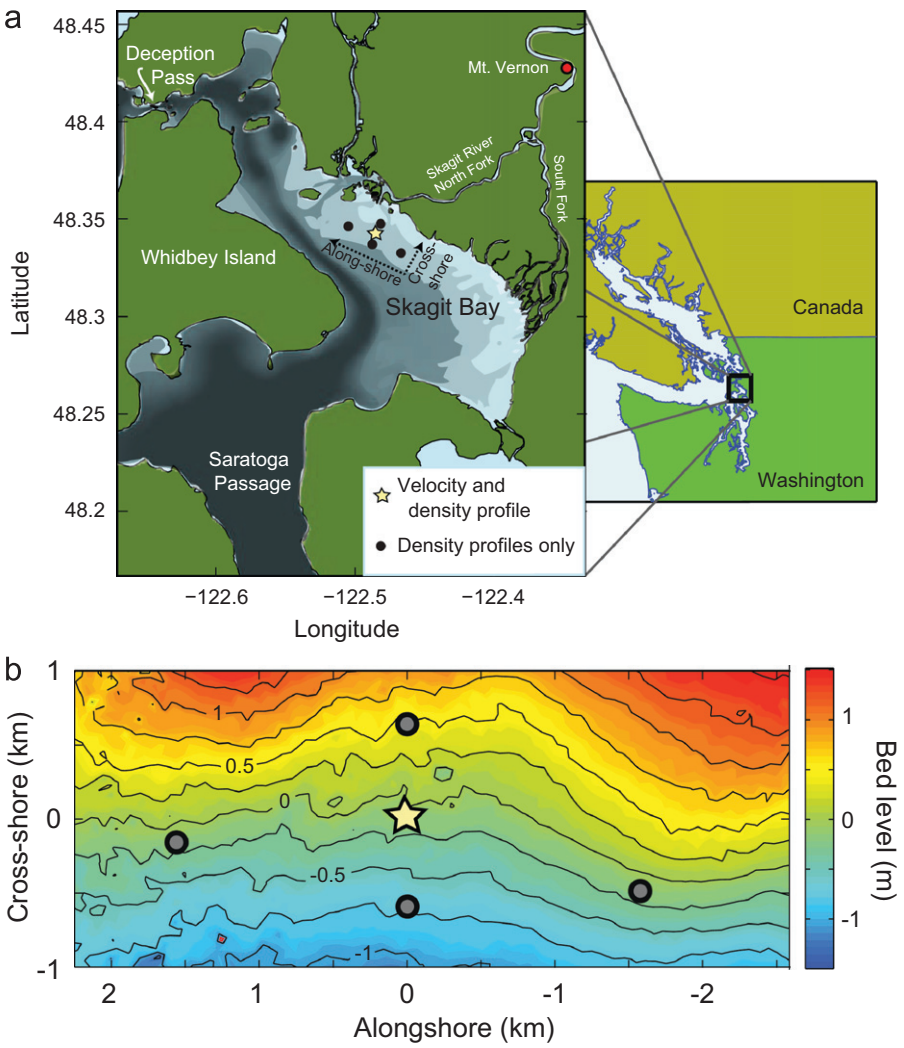


**Fig. 1.** (a) Map of Skagit Bay and surrounding area (from NOAA/NOS Medium Resolution Coastline Database) and instrument array (black circles and yellow star indicate where density profiles and colocated velocity and density profiles, respectively, were obtained). Bottom pressure (and water depth) was measured at all instrument locations. Bathymetric contours are shown in four shades of gray, with the darkest areas being the deepest waters in Saratoga Passage, in Skagit Bay along Whidbey Island, and in Deception Pass. The north fork river channel is shown in medium-dark gray, and the shallowest areas of the tidal flats are light blue–gray. The smaller map (NOAA World Vector Shoreline Database) on the right shows the location of Skagit Bay on the Pacific Northwest coast. Positive cross-shore is toward the northeast and positive alongshore is toward the northwest. (b) Bathymetry (relative to NAVD88, contours every 0.5 m, color bar on right) as a function of cross- and alongshore position on the tidal flats surrounding the instruments (note: the maximum water depth at the 0 m contour is about 3 m). (For interpretation of the references to color in this figure legend, the reader is referred to the web version of this article.)

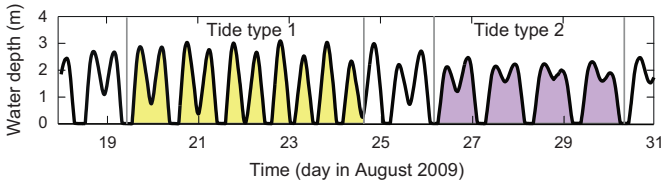


**Fig. 2.** Water depth versus time at the central sensor location with type 1 and type 2 tides shaded in yellow and purple, respectively. (For interpretation of the references to color in this figure legend, the reader is referred to the web version of this article.)

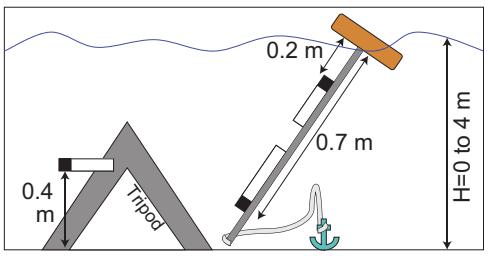


**Fig. 3.** Schematic of the fixed CT (mounted on a tripod) and the floating assembly with CT and CTD sensors.

differences between the 512-s averaged densities from individual CT measurements and the average of the values from all sensors at the same elevation were about 2 kg/m$^3$, or about 25% of the surface-to-bottom density difference. Differences between the sensor-averaged density and the measurement at the central location for the lower floating CTD sensor also were about 2 kg/m$^3$. Results were similar for averages including data from only the alongshore (on the same depth contour) or only the cross-shore sensors. Atmospheric pressure was removed from measured bottom pressures. The corrected pressures were averaged over 512 s, and used to estimate water levels assuming hydrostatic pressure and using water density measured by the CT sensors. Pressure drifts were then removed by subtracting a quadratic fit to low-tide data, when the flat was dry and the water depth should have been

Please cite this article as: Pavel, V., et al., Processes controlling stratification on the northern Skagit Bay tidal flats. Continental Shelf Research (2012), http://dx.doi.org/10.1016/j.csr.2012.06.012

negligible. ADVs were assumed to be fouled or out of the water, and data were discarded when the signal strength was low or when the flows were noisy (defined as times when the root-mean-square velocity fluctuations were more than twice the fluctuations expected from applying linear theory to the pressure signal). Flows measured with ADVs were averaged over 512 s, ignoring any points where the data were discarded. The estimated water levels were used to determine when profiler bins were above the water surface. Current profiles based on profiler data were averaged over 600-s periods, then interpolated in time and output every 512 s to combine with ADV data.

Density is dominated by salinity, which ranges from fresh river water (density $\sim$1000 kg/m$^3$) to Puget Sound water with salinity 28 PSU (density $\sim$1020 kg/m$^3$). Cross-shore and alongshore density gradients had median values of $\sim 5\times10^{-3}$ and $\sim 5\times10^{-4}$ kg/m$^4$, respectively. Maximum water depths ranged from $\sim$4 m at the most offshore sensor to $\sim$2 m at the most onshore sensor. Maximum values of cross- and alongshore velocity were $\sim$0.5 m/s.

Similar to prior observations of salt-wedge estuaries (Ralston et al., 2010; Giddings et al., 2011) and numerical simulations of Skagit Bay (Yang and Khangaonkar, 2009), the water column is fresh at the beginning of flood tide, just after the tidal flat is submerged (Fig. 4). The salinity front moves onshore during flood, with the water column becoming increasingly saline. During ebb, the salinity front moves offshore and the water freshens while draining off the tidal flats.

During type 1 tides, cross- and alongshore velocities (Fig. 5a and c) have similar magnitudes (see also Webster et al., submitted for publication). Although cross-shore flows are relatively weak during type 2 tides (Fig. 5b), alongshore flows are large (Fig. 5d), resulting in similar total flow magnitudes during springs and neaps.

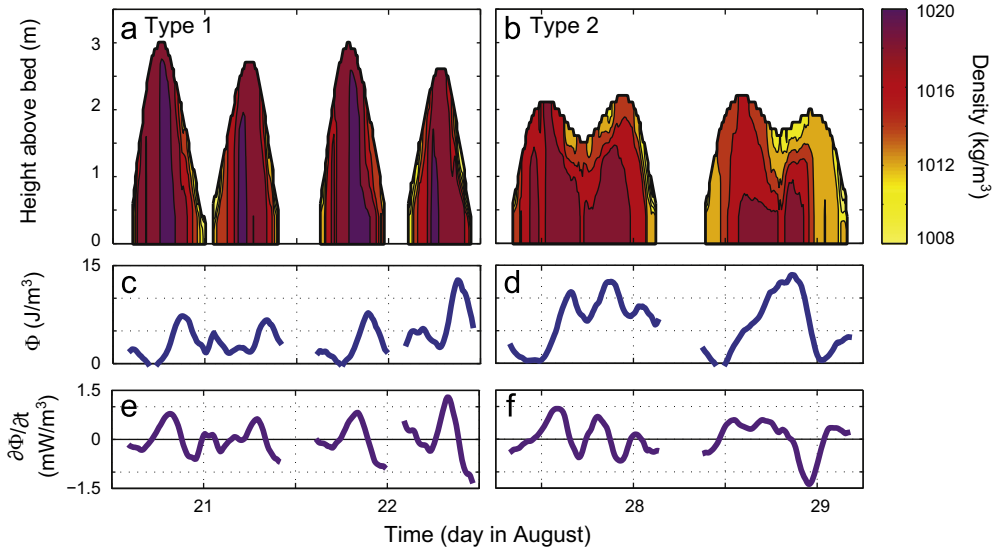


**Fig. 4.** (a and b) Water density (color contours) as a function of depth (thick black curve) and time, and (c and d) $\Phi$ and (e and f) $\partial\Phi/\partial t$ vs. time for type 1 (a, c, and e) and type 2 (b, d, and f) tides.

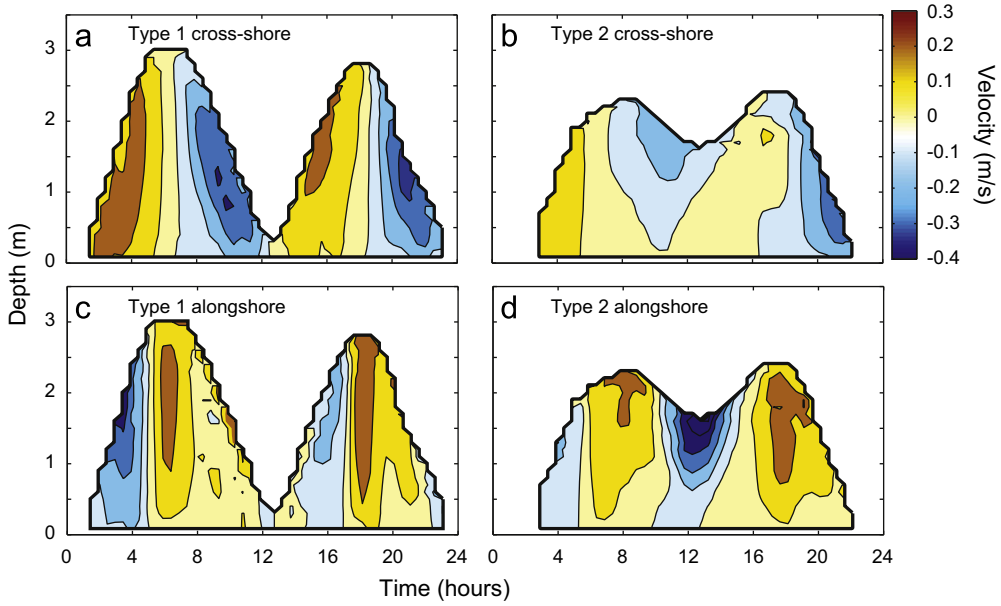


**Fig. 5.** Phase-averaged (a and b) cross- and (c and d) alongshore velocity (color contours) as a function of depth (thick black curve) and time for type 1 (a and c) and type 2 (b and d) tides.

Please cite this article as: Pavel, V., et al., Processes controlling stratification on the northern Skagit Bay tidal flats. Continental Shelf Research (2012), http://dx.doi.org/10.1016/j.csr.2012.06.012

## 3. Theory and processing

### 3.1. Theory

The stratification is quantified using the potential energy anomaly ($\Phi$), the amount of energy per unit volume required to homogenize the water column:

$$\Phi = -\frac{g}{D}\int_{-h}^{\eta} \rho' z dz, \tag{1}$$

where $g$ is the gravitational acceleration, $h$ and $\eta$ are the mean depth and the elevation of the surface above the mean, $D=h+\eta$ is the total water depth, $\rho=\overline{\rho}+\rho'$ is the density, where $\overline{\rho}$ and $\rho'$ are the depth-mean and residual values, and $z$ is the vertical coordinate, which is zero at the mean surface and positive upward. During the study, $\Phi$ ranged from 0 to 15 J/m$^3$. Errors in the density estimated at the upper CT sensor at the central location could result in up to ~10% errors in the potential energy anomaly.

The temporal evolution of $\Phi$ (Fig. 4) is given by (Burchard and Hofmeister 2008):

$$\begin{aligned}\frac{\partial \Phi}{\partial t} = &-\nabla_h(\overline{\mathbf{u}}\Phi) + \frac{g}{D}\nabla_h\overline{\rho}\cdot\int_{-h}^{\eta}\mathbf{u}' z dz - \frac{g}{D}\int_{-h}^{\eta}\left(\eta-\frac{D}{2}-z\right)\mathbf{u}'\cdot\nabla_h\rho' dz\\ &-\frac{g}{D}\int_{-h}^{\eta}\left(\eta-\frac{D}{2}-z\right)w'\frac{\partial\rho'}{\partial z}dz + \frac{g}{D}\int_{-h}^{\eta}K_\nu\frac{\partial\rho}{\partial z}dz - \frac{\rho_0}{2}\left(P_b^s+P_b^b\right)\\ &+\frac{g}{D}\int_{-h}^{\eta}\left(\eta-\frac{D}{2}-z\right)Q dz + \frac{g}{D}\int_{-h}^{\eta}\left(\eta-\frac{D}{2}-z\right)\nabla_h(K_h\nabla_h\rho)dz\end{aligned} \tag{2}$$

where $t$ is time, $\nabla_h$ indicates the horizontal components of the gradient operator, $\overline{\mathbf{u}}$ is the horizontal velocity vector where the overbar denotes the depth-average and the prime is the deviation from the depth-average, $\rho_0$ is a reference density, $P_b^s$ and $P_b^b$ are surface and bottom buoyancy fluxes, respectively, $Q$ represents inner sinks and sources, $K_h$ is the horizontal eddy diffusivity, and $w'$ is the deviation of the vertical velocity ($w$) from a linear profile:

$$w' = w - \left[\left(\frac{\partial\eta}{\partial t}+\overline{\mathbf{u}}\cdot\nabla_h\eta\right)\frac{z+h}{D} - \overline{\mathbf{u}}\cdot\nabla_h h\frac{\eta-z}{D}\right]. \tag{3}$$

The eddy diffusivity $K_\nu$ is estimated as (Munk and Anderson, 1948; Nepf and Geyer, 1996; Burchard and Hofmeister, 2008; Becker et al., 2009):

$$K_\nu = K_0(1+3.33R_i)^{-3/2} \tag{4}$$

where $R_i$ is the bulk Richardson number (Byun and Wang, 2005; Stacey and Ralston, 2005) and $K_0$ is the estimated eddy diffusivity for an unstratified water column (see Appendix for further details on the mixing parameterization). The last three terms on the right side of Eq. (2) are expected to be small compared with the other terms and are neglected. To examine the effects of changing depth, the first term is separated into an advection and depth change term:

$$-\nabla_h(\overline{\mathbf{u}}\Phi) = -\overline{\mathbf{u}}\nabla_h\Phi - \Phi\nabla_h\overline{\mathbf{u}}. \tag{5}$$

From continuity, the horizontal gradient of the mean velocity can be expressed in terms of depth changes, as

$$\nabla_h\overline{\mathbf{u}} = -\frac{1}{D}\left(\frac{\partial\eta}{\partial t}+\overline{\mathbf{u}}\cdot\nabla_h D\right). \tag{6}$$

Rearranging the integrals as

$$-\int_{-h}^{\eta}\left(\eta-\frac{D}{2}-z\right)\chi dz = \int_{-h}^{\eta} z(\chi-\overline{\chi})dz = \int_{-h}^{\eta} z\chi' dz \tag{7}$$

where $\chi$ is an arbitrary depth-dependent function, the overbar denotes the depth-average, and the prime denotes the deviation from the depth-average, results in

$$\begin{aligned}\frac{\partial\Phi}{\partial t} = &\underbrace{-\overline{\mathbf{u}}\cdot\nabla_h\Phi}_{A} + \underbrace{\frac{\Phi}{D}\left(\frac{\partial\eta}{\partial t}+\overline{\mathbf{u}}\cdot\nabla_h D\right)}_{DC} + \underbrace{\frac{g}{D}\nabla_h\overline{\rho}\cdot\int_{-h}^{\eta}\mathbf{u}' z dz}_{DS}\\ &+\underbrace{\frac{g}{D}\int_{-h}^{\eta}\left(\mathbf{u}'\cdot\nabla_h\rho'\right)' z dz}_{NS} + \underbrace{\frac{g}{D}\int_{-h}^{\eta}K_\nu\frac{\partial\rho}{\partial z}dz}_{M} + \underbrace{\frac{g}{D}\int_{-h}^{\eta}\left(w'\frac{\partial\rho}{\partial z}\right)' z dz}_{VA}\end{aligned} \tag{8}$$

where term $A$ is horizontal advection, $DC$ is the effect of depth changes in both time and space, $DS$ is depth-mean straining, $NS$ is non-mean straining caused by shear acting on a non-depth-uniform density gradient, $M$ is mixing, and $VA$ is vertical advection shifting the isopycnals up and down.

### 3.2. Processing

To evaluate the integrals in Eq. (8), density and velocity profiles were linearly interpolated onto a 0.1-m vertical grid. Profiles were extended to the surface and bed assuming constant values given by the highest and lowest measurement, respectively. Comparisons of $\Phi$ estimated by linearly interpolating the vertically sparse density measurements with $\Phi$ estimated with a two-layer model using the densities at the upper and lower sensors suggest errors are of order 10%. Results are similar to assuming zero flux at the bed and surface and using a linear extrapolation of the vertical gradient. Near-bottom density was interpolated linearly along the sloping bed. The vertical structure of cross-shore density gradients at elevations between the bed levels at any two locations was calculated using the density profile at the deeper location and the corresponding near-bottom density at the same elevation (Fortunato and Baptista, 1996). Horizontal gradients were evaluated using upstream differences (determined from the depth-averaged velocity at the central location).

Profiler measurements of horizontal flows coupled with a mass balance suggest that vertical velocities ($w$) were smaller than the resolution of the instrument (0.001 m/s), so the vertical advection term could not be calculated from data. Previous results suggest that this term is unlikely to be large except in a small region near the density front (Nepf and Geyer, 1996; Burchard and Hofmeister, 2008; de Boer et al., 2008; Hofmeister et al., 2009; Marques et al., 2010), and thus it is neglected here. However, vertical advection may contribute to the errors in the estimated stratification balance (Eq. (8)).

The water depth, $\Phi$, and all terms in Eq. (8) were smoothed using a 7200-s running average. The averaging period was chosen to be shorter than 1/4-tidal period to resolve tidal fluctuations, but longer than the advective timescale between sensor locations (about 3600 s and 4800 s in the cross- and alongshore, respectively). This temporal averaging and smoothing reduces errors owing to unresolved small-scale spatial variability. $\Phi$ was smoothed before difference calculations were performed, and the results were smoothed again after computing $\partial\Phi/\partial t$ and the advection term. All terms were phase averaged over 24-h long (diurnal) cycles for type 1 (5 cycles) and type 2 (4 cycles) tides. Correlation coefficients between $\Phi$ for individual tidal cycles and the ensemble-averaged $\Phi$ are greater than 0.9, indicating that the ensemble averages are representative of the tidal processes.

## 4. Results

### 4.1. The potential energy anomaly balance

The ensemble-averaged diurnal variations of $\partial\Phi/\partial t$ (Fig. 6), including the timing of the maxima and minima, are consistent

Please cite this article as: Pavel, V., et al., Processes controlling stratification on the northern Skagit Bay tidal flats. Continental Shelf Research (2012), http://dx.doi.org/10.1016/j.csr.2012.06.012

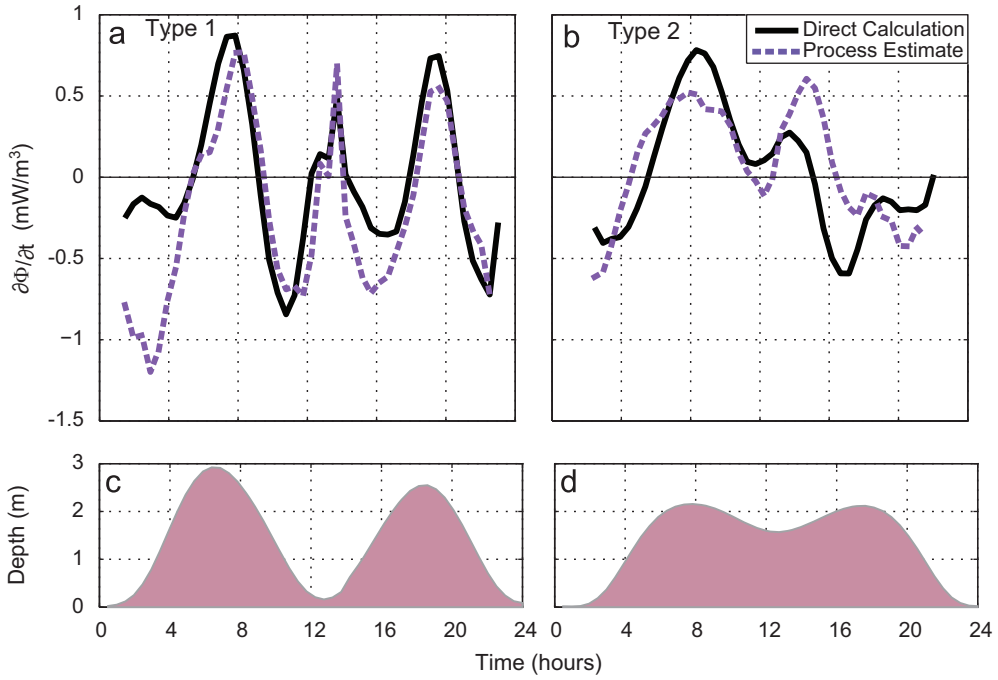


**Fig. 6.** Phase-averaged $\partial\Phi/\partial t$ based on the observed density profiles (solid black curves) and on estimations of stratification-related processes (right-hand side of Eq. (1), dotted purple curves) versus time for (a) type 1 and (b) type 2 tides. Squared correlations between the direct and process estimates are about 0.7. The shaded areas (c and d) show the relative water depth during each tidal cycle. (For interpretation of the references to color in this figure legend, the reader is referred to the web version of this article.)

with the stratification balance (Eq. (8)). The good agreement between the left and right side of the balance suggests that the sum of the neglected terms (including vertical advection) is not large compared with the retained terms, possibly because the neglected terms cancel, as in numerical simulations of the Patos Lagoon ROFI (Marques et al., 2010).

During the type 1 and 2 strong flood tides following the biggest low tide (when the tidal flat is dry), the thin layer of water initially submerging the flats is slightly stratified (Fig. 4c and d), but becomes increasingly well mixed (Fig. 4e and f, $\partial\Phi/\partial t < 0$). In contrast, during the type 1 flood following the smaller low tide, the stratification increases sharply (Fig. 6a time ~12–14 h), consistent with cross-shore transport of strong density fronts (de Boer et al., 2008; Wang et al., 2009; Giddings et al., 2011). Similar to observations in strongly forced salt-wedge estuaries (Ralston et al., 2010a; Giddings et al., 2011), maximum stratification occurs at about mid ebb tide (Fig. 6a time ~9 and ~21 h, where $\partial\Phi/\partial t$ changes from positive to negative). This mid-ebb maximum distinguishes the tidal flats from partially mixed estuaries and ROFIs in which depth-mean straining dominates and maximum stratification occurs during late ebb or low water (Nepf and Geyer, 1996; Rippeth et al., 2001; Burchard and Hofmeister, 2008). During type 2 tides, stratification continues to increase during the weak ebb, the smaller low, and the beginning of the weak flood (Fig. 6b, time from ~8–16 h, $\partial\Phi/\partial t > 0$). However, in contrast to prior studies (Ralston and Stacey, 2005b; Wang et al., 2009; Ralston et al., 2010; Giddings et al., 2011), the stratification decreases from about mid weak flood through the second high tide and the following strong ebb (Fig. 6b time ~16–22 h).

The individual terms in the balance (Fig. 7) indicate which processes dominate the stratification. The freshwater draining off the flats during the strong ebbs remains partly stratified (Figs. 4c and d). Thus, on the strong floods, advection and depth-mean straining (solid blue and dashed purple curves in Fig. 7a for time ~2–6 and ~12–16 h, and Fig. 7b for time ~2–6 h) often are

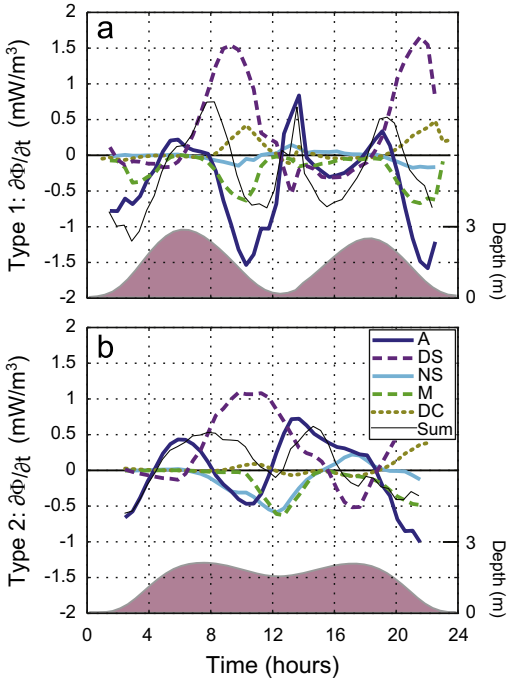


**Fig. 7.** Phase-averaged values of terms on the right side of Eq. (8) (colored curves, see legend) and the sum of the terms (thin black curves, e.g., same as the dotted purple curves in Fig. 6) versus time for (a) type 1 and (b) type 2 tides. The shaded areas show the water depth (axis on right) during a tidal cycle. (For interpretation of the references to color in this figure legend, the reader is referred to the web version of this article.)

negative as the thin, mostly fresh tongue that initially covers the flats is replaced by water from offshore that is increasingly well-mixed and saline. Advection usually opposes the positive depth-mean straining on the ebb (Fig. 7 time ~8–12 and ~18–22 h),

Please cite this article as: Pavel, V., et al., Processes controlling stratification on the northern Skagit Bay tidal flats. Continental Shelf Research (2012), http://dx.doi.org/10.1016/j.csr.2012.06.012

indicating that the freshwater that is trapped near the shore at high tide is less stratified than the offshore water, similar to many estuaries (Burchard and Hofmeister, 2008; Ralston et al., 2010; Giddings et al., 2011), but in contrast to models of ROFIs (de Boer et al., 2008). The negative advection also suggests that stratified water is transported to the offshore flats during the strong ebb, where it would be transported northward towards Deception Pass. Comparison of the terms during type 1 tides with those during type 2 tides suggests that large negative values of $\partial\Phi/\partial t$ occur on strong (but not weak) ebbs at least partly because advection of well-mixed water is larger on strong ebbs (compare the maximum negative values of the dark blue curve in Fig. 7a with those in Fig. 7b, e.g., near time 10 h).

During type 2 tides, $\partial\Phi/\partial t$ remains positive throughout the weak ebb and the beginning of the weak flood (Fig. 6b), indicating continually increasing stratification, in contrast to observations of the Snohomish River estuary (Wang et al., 2009; Giddings et al., 2011) that show slight weakening of the stratification during this period owing to local mixing dominating over weak advection and straining. Here, near the end of the type 2 weak ebb, advection is small and switches from negative to positive (blue curve in Fig. 7b near time about 12 h), at least partly owing to positive alongshore advection (Fig. 8b) caused by strong south-easterly alongshore flows (Fig. 5d) transporting stratified water alongshore from the north fork of the Skagit River towards the instrument location, and ultimately towards the central flats and Saratoga Passage. The water on the offshore flats remains stratified following the weak ebb, and thus cross-shore advection is positive throughout the weak flood. Cross-shore depth-mean straining also remains positive during the small low and until about mid weak flood (Fig. 7b) owing to vertically sheared currents with offshore flow near the surface (Fig. 5b).

Mixing (Fig. 7, green dashed curve), which always is negative (reducing stratification), is largest when internal or bottom shear is large and when the water is not well mixed already. During type 1 tides, mixing is strongest during the ebbs, which is consistent with the combined interfacial- and bottom-generated mixing observed in strongly forced salt-wedge estuaries (Ralston et al., 2010b; Giddings et al., 2011; Wang et al., 2011). Mixing is weak during floods despite strong nearbed flows primarily because the water column already is well mixed. During type 2 tides, mixing is large during the small low tide (dashed green curve in Fig. 7b for time about 12 h), similar to observations and model predictions in the Snohomish estuary (Wang et al., 2009; Giddings et al., 2011). Nearbed flows are weak, while mid-water-column shear is strong (Fig. 5b and d), suggesting the mixing on type 2 tides primarily is caused by internal shear, especially for the more highly vertically sheared alongshore currents (Fig. 5d). Similar to other systems with strong stratification (Burchard and Hofmeister, 2008; de Boer et al., 2008), mixing usually is smaller than advection and depth-mean straining (Fig. 7b), but here mixing remains significant owing to the shallow depths.

The non-mean straining is small during type 1 tides (Fig. 7a, solid light blue curve). However, in contrast to numerical simulations suggesting that non-mean straining is large only near the river or estuarine mouth (de Boer et al., 2008; Marques et al., 2010), here non-mean straining is similar in magnitude to the other terms during type 2 tides (Fig. 7b), and it reduces the increase in stratification during the small low tide (Fig. 6b, $\partial\Phi/\partial t > 0$) and the decrease in stratification during the latter half of the weak flood (Fig. 6b, $\partial\Phi/\partial t < 0$). The prior simulations suggest vertical advection may balance non-mean straining, and thus the discrepancies between the direct- and process-based estimates of $\partial\Phi/\partial t$ (Fig. 6b) during the small low tide and weak flood may result partly from neglecting vertical advection.

Similar to long, narrow estuaries (Simpson et al., 1990; Nepf and Geyer, 1996; Burchard and Hofmeister, 2008; Giddings et al., 2011), the cross-shore advection (Fig. 8a) and depth-mean straining (Fig. 8c) during type 1 tides are 5 and 15 times larger, respectively, than the alongshore components. However, the

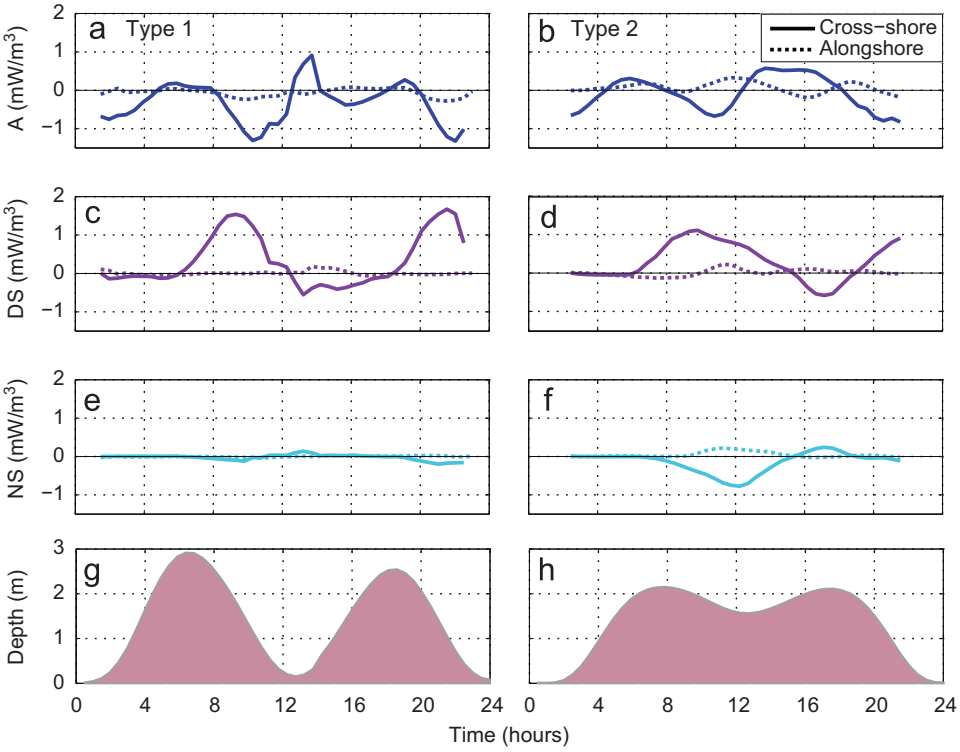


**Fig. 8.** Phase-averaged cross- (solid curves) and alongshore (dotted curves) components of (a and b) advection, (c and d) depth-mean straining, and (e and f) non-mean straining for (a, c, and e) type 1 and (b, d, and f) type 2 tides versus time. The shaded areas (g and h) show the relative water depth during a tidal cycle.

Please cite this article as: Pavel, V., et al., Processes controlling stratification on the northern Skagit Bay tidal flats. Continental Shelf Research (2012), http://dx.doi.org/10.1016/j.csr.2012.06.012

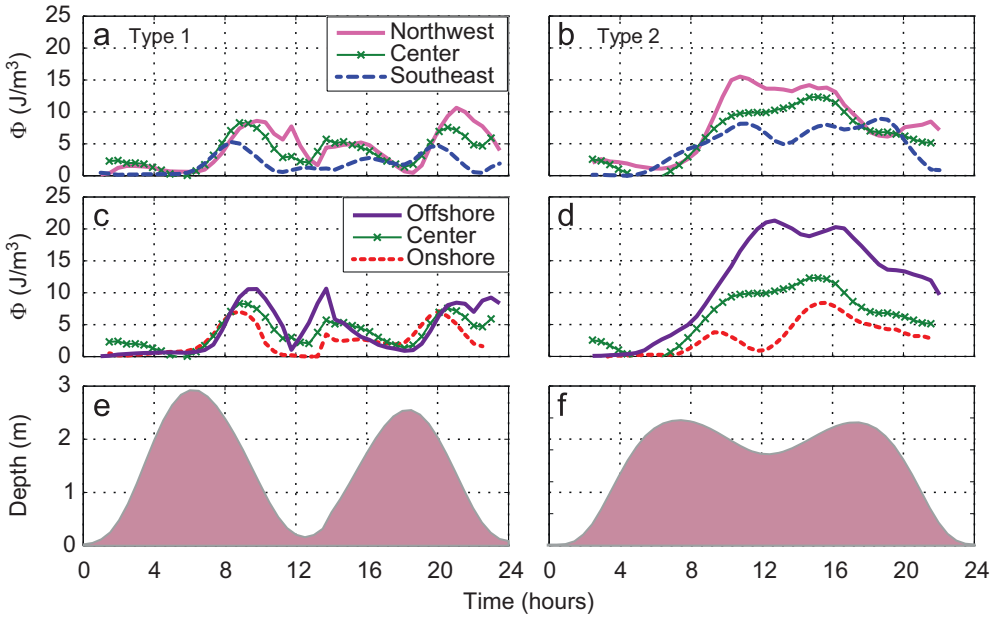


**Fig. 9.** Phase-averaged potential energy anomaly for (a and b) alongshore and (c and d) cross-shore sensor lines for (a and c) type 1 and (b and d) type 2 tides. The shaded areas (e and f) show the relative water depth during a tidal cycle.

cross- and alongshore velocities (Fig. 5a and c) have similar magnitudes, suggesting the dominance of cross-shore processes is a result of larger cross-shore density gradients. The depth-mean (Fig. 8d) and non-mean (Fig. 8f) straining also are dominated by the cross-shore component during type 2 tides, but the alongshore component of the advection has about half the magnitude of its cross-shore component (Fig. 8b). The largest magnitudes of alongshore advection for type 2 tides result from large alongshore stratification variations (Fig. 9b time from 10 to 16 h) and alongshore-dominated flows (compare Fig. 5d with 5b for time from 10 to 16 h) during the end of the weak ebb and the beginning of the weak flood owing to the large-scale tidal circulation (Yang and Khangaonkar, 2009).

### 4.2. Spatial variability

As in prior studies (Burchard and Hofmeister, 2008; de Boer et al., 2008; Marques et al., 2010), the potential energy anomaly and the dominant processes controlling the stratification can be spatially variable (Fig. 9). Here, the strength of the stratification typically increases towards the northwest (towards the mouth of the north fork, Fig. 9a and b) and offshore (Fig. 9c and d). For both type 1 and 2 tides, the local maxima in stratification occurs earlier at onshore locations (red dotted curves in Fig. 9c and d) than at offshore locations (purple solid curves), possibly owing to the earlier passage of the density front.

During type 1 tides, temporal changes in $\Phi$ are similar at all sensors (Fig. 9a and c), in contrast to larger, more spatially variable estuaries and ROFIs (de Boer et al., 2008; Burchard and Hofmeister, 2008; Wang et al., 2009; Marques et al., 2010, 2011; Ralston et al., 2010a; Giddings et al., 2011). The stratification maximum on the flood following the smaller low becomes stronger at the northwest (closer to the north fork, Fig. 9a for time about 20 to 24 h) and offshore (Fig. 9c for time about 20 to 24 h) locations, possibly because the salt wedge becomes stronger closer to the river mouth and offshore.

The maximum stratification is larger during type 2 tides than during type 1 tides at most locations (Fig. 9). Consistent with prior observations in shallow channels and in strongly forced salt-wedge estuaries (Ralston and Stacey, 2005b; Wang et al., 2009; Ralston et al., 2010; Giddings et al., 2011), the water column remains stratified during the type 2 small low tide, except at the most onshore location (Fig. 9d). The stratification increases during the weak flood at most locations (Fig. 9b and d), presumably owing to the same alongshore advection of stratified water (Fig. 8b) and depth-mean straining (Fig. 6b) observed at the central location. Except at the southeastern and onshore locations, the water column remains partly stratified until water drains off the flat.

The spatially uniform temporal evolution of stratification during type 1 tides suggests that the processes affecting stratification are similar across the flats. However, the spatial variability during type 2 tides suggests that different processes may dominate depending on location, similar to numerical model simulations over large regions of salt-wedge estuaries (Wang et al., 2009; Ralston et al., 2010), and to ROFIs (Marques et al., 2010) and numerical simulations of the Skagit flats (Pavel, 2012). The latter show that the ratio of alongshore to cross-shore advection and straining ranges from near 0 on the southern flats to greater than 1 near the north fork.

## 5. Summary and conclusions

The stratification observed on the shallow and wide tidal flats near the north fork of the Skagit River has similarities to deep-water nearshore regions of freshwater influence (ROFIs) where strong flows are perpendicular to the density gradient (Rippeth et al., 2001; de Boer et al., 2008; Marques et al., 2010, 2011), and to narrow tidal-flat channels (Ralston and Stacey, 2005a,b) and strongly forced salt-wedge estuaries (Wang et al., 2009; Ralston et al., 2010a,b; Giddings et al., 2011) where tidal flows and density gradients are aligned.

Type 1 tidal processes are roughly described as a salt wedge with a nearly vertical front that is transported onshore on the flood tide, and that is strained so it covers a larger area while it is advected offshore on the ebb. The water on the tidal flats does not become completely mixed during the strong ebb, and thus the initial tongue of water crossing the flats on strong floods often is partly stratified. As in prior studies, the water becomes increasingly saline during the

Please cite this article as: Pavel, V., et al., Processes controlling stratification on the northern Skagit Bay tidal flats. Continental Shelf Research (2012), http://dx.doi.org/10.1016/j.csr.2012.06.012

strong flood, and for these nearly semi-diurnal tides, the maximum stratification occurs during mid ebb tide. The changes in stratification result primarily from cross-shore tidal straining and advection. The strong alongshore flows did not contribute significantly to the stratification, at least partly because alongshore density and stratification gradients were small when flows were strong.

During type 2 tides, the salt wedge again passes onto the flats during the strong flood, but stratification increases during the prolonged high water of the weak ebb and flood. In contrast to prior estuarine studies, but similar to many ROFIs, alongshore flows (roughly parallel to isopycnals) are stronger than cross-shore flows, and alongshore gradients in stratification are large. Thus, the increased stratification is partly owing to alongshore advection of stratified water from the north fork of the Skagit River, as well as to strongly sheared cross-shore flows that remain offshore-directed at the surface until mid weak flood, when stratification is maximum. In addition, flows are relatively weak (compared with the strong ebb and flood of type 1 tides), and mixing is minimal. Thus, stratification processes on tidal flats may have similarities to ROFIs, as well as to salt-wedge estuaries, particularly in areas with mixed tides that have prolonged periods of high water and weak flows (which may lead to alongshore inhomogeneous stratification near freshwater sources).

These results suggest that

- stratification processes may be primarily cross-shore on many tidal flat systems, especially if the flows are dominated by strong floods and ebbs with significant mixing, but
- alongshore processes may be important to stratification in systems with alongshore-inhomogeneous freshwater input and a prolonged period of high water (and thus weak flows and mixing).

In addition, the large advection terms suggest strong fronts are moved across and along the flats. Positive straining (indicating generation of stratification) usually is larger than negative mixing (indicating destruction of stratification), suggesting water that becomes stratified near the measurement location is either mixed elsewhere on the flats, or exported to the surrounding basins.

Temporal changes in stratification are similar across and along the flats in this region. However, stratification increases offshore and alongshore towards the north fork (the river mouth closest to the instruments).

## Acknowledgments

We thank T.H.C. Herbers and J. MacMahan for providing current profilers, and W. Boyd, S. Burnet, D. Darnell, D. Giffen, L. Gorrell, S. Kilgallin, E. Ladouceur, L. Siegel, E. Williams, R. Yopak, and S. Zippel for helping obtain the field observations. The Office of Naval Research, the National Science Foundation, a National Security Science and Engineering Faculty Fellowship, and the PADI Foundation provided support.

## Appendix. Mixing parameterization

The mixing term $M$ in the stratification balance uses a common parameterization of the vertical buoyancy flux (Nepf and Geyer, 1996; Becker et al., 2009; Ralston et al., 2010) based on the eddy diffusivity $K_\nu$. The eddy diffusivity is estimated using parameterizations of the turbulence produced in the bottom boundary layer modified by the ability of stratified flow to support turbulence (Munk and Anderson, 1948). The eddy diffusivity was calculated by $K_\nu = K_0(1+3.33R_i)^{-3/2}$, where $K_0$ is the estimated eddy diffusivity for an unstratified water column and $R_i$ is the bulk Richardson number. Extending a boundary layer method (Becker et al., 2009) developed for weakly stratified regions, $K_0$ is calculated by $K_0 = 0.4C_0u_*z_b(1-(z_b/D))$, where the scaling factor $C_0$ is included to account for the strongly stratified conditions and is set equal to 0.1 based on a fit to the stratification balance and to model predictions of $K_\nu$ (Ralston et al., in this issue), $u_*$ is the friction velocity, $z_b$ is the smaller of the height above the bed or the thickness of the bottom boundary layer, and $D$ is the total water depth. An isotropic estimate is used for the friction velocity, given by $u_*^2 = C_d(\overline{u}^2+\overline{v}^2)$, where $\overline{u}$ and $\overline{v}$ are the depth-averaged cross- and alongshore velocities, respectively, and the drag coefficient $C_d$ is 0.001. The data collection methods did not allow for more accurate estimates of the friction velocity by direct measurement of turbulence. The Richardson number is calculated by $R_i = (gD/\overline{\rho})\Delta\rho/((\Delta u)^2+(\Delta v)^2)$, where $g$ is gravitational acceleration, $\overline{\rho}$ is the depth-averaged density, and $\Delta\rho$, $\Delta u$, $\Delta v$ are the maximum difference in density, cross-shore velocity, and alongshore velocity, respectively (Byun and Wang, 2005). The thickness of the bottom boundary layer ($H_{BBL}$) is estimated by $H_{BBL} = u_*\left((g/\overline{\rho}R_i)(\partial\overline{\rho}/\partial x)\right)^{-1/2}$ (Stacey and Ralston, 2005).

Alternate methods evaluated for the mixing parameterization include a constant and uniform $K_\nu$, a depth-varying gradient $R_i$ calculated by $R_i = (g/\overline{\rho})(\delta\rho_i/\delta z)\left[(\delta u_i/\delta z)^2+\left((\delta v_i/\delta z)\right)^2\right]^{-1}$, a constant and uniform $K_0$, a depth-uniform $K_0$ calculated by $K_0 = 0.4C_0u_*(D/10)$, and combinations thereof. Unrealistic values of $R_i$ are obtained when calculated in a depth-varying manner owing to the constant extrapolation method used to obtain density and velocity values throughout the water column. Constant and uniform $K_0$ and $K_\nu$ were rejected because they do not consider the effects of stratification and flow speed. The choice of the method used was based on the best fit of the total dynamic balance.

## References

Banas, N.S., Hickey, B.M., MacCready, P., Newton, J.A., 2004. Dynamics of Willapa Bay, Washington: a highly unsteady, partially mixed estuary. Journal of Physical Oceanography 34 (11), 2413–2427.

Becker, M.L., Luettich, R.A., Seim, H., 2009. Effects of intratidal and tidal range variability on circulation and salinity structure in the Cape Fear River Estuary, North Carolina. Journal of Geophysical Research 114 (C4), C04006, http://dx.doi.org/10.1029/2008JC004972.

Blanton, J.O., Lin, G., Elston, S.A., 2002. Tidal current asymmetry in shallow estuaries and tidal creeks. Continental Shelf Research 22, 1731–1743.

Burchard, H., Hofmeister, R., 2008. A dynamic equation for the potential energy anomaly for analysing mixing and stratification in estuaries and coastal seas. Estuarine, Coastal and Shelf Science 77 (4), 679–687, http://dx.doi.org/10.1016/j.ecss.2007.10.025.

Byun, D.S., Wang, X.H., 2005. The effect of sediment stratification on tidal dynamics and sediment transport patterns. Journal of Geophysical Research 110 (C3), C03011, http://dx.doi.org/10.1029/2004JC002459.

Chant, R.J., Stoner, A.W., 2001. Particle trapping in a stratified flood-dominated estuary. Journal of Marine Research 59, 29–51.

Chen, S.N., Geyer, W.R., Sherwood, C.R., Ralston, D.K., 2010. Sediment transport and deposition on a river-dominated tidal flat: an idealized model study. Journal of Geophysical Research 115, C10040, http://dx.doi.org/10.1029/2010JC006248.

Cheng, P., Wilson, R.E., Chant, R.J., Fugate, D.C., Flood, R.D., 2009. Modeling influence of stratification on lateral circulation in a stratified estuary. Journal of Physical Oceanography 39, 2324–2337, http://dx.doi.org/10.1175/2009JPO4157.1.

de Boer, G.J., Pietrzak, J.D., Wenterwerp, J.C., 2008. Using the potential energy anomaly equation to investigate tidal straining and advection of stratification in a region of freshwater influence. Ocean Modelling 22 (1-2), 1–11, http://dx.doi.org/10.1016/j.ocemod.2007.12.003.

Elgar, S., Raubenheimer, B., 2011. Currents in a small sandy tidal channel. Continental Shelf Research 31, 9–14, http://dx.doi.org/10.1016/j.csr.2010.10.007.

Fan, D.D., Guo, Y.X., Wang, P., Shi, J.Z., 2006. Cross-shore variations in morphodynamic processes of an open-coast mudflat in the Changjiang Delta, China: with

an emphasis on storm impacts. Continental Shelf Research 26 (4), 517–538, http://dx.doi.org/10.1016/j.csr.2005.12.011.
Fortunato, A.B., Baptista, A.M., 1996. Evaluation of horizontal gradients in sigma-coordinate shallow water model. Atmosphere-Ocean 34 (3), 489–514.
Fortunato, A.B., Baptista, A.M., Luettich, R.A., 1997. A three-dimensional model of tidal currents in the mouth of the Tagus estuary. Continental Shelf Research 17 (14), 1689–1714.
Fortunato, A.B., Oliviera, A., Baptista, A.M., 1999. On the effect of tidal flats on the hydrodynamics of the Tagus estuary. Oceanologica Acta 22 (1), 31–44.
Friedrichs, C.T., Aubrey, D.G., 1988. Non-linear tidal distortion in shallow well-mixed estuaries: a synthesis. Estuarine, Coastal and Shelf Science 27 (5), 521–545.
Geyer, W.R., Farmer, D.M., 1989. Tide-induced variation of the dynamics of a salt wedge estuary. Journal of Physical Oceanography 19, 1060–1072.
Giddings, S.N., Fong, D.A., Monismith, S.G., 2011. Role of straining and advection in the intratidal evolution of stratification, vertical mixing, and longitudinal dispersion of a shallow, macrotidal, salt wedge estuary. Journal of Geophysical Research 116 (C3), C03003, http://dx.doi.org/10.1029/2010JC006482.
Grossman, E.E., Stevens, A., Gelfenbaum, G., Curran, C., 2007. Nearshore circulation and water column properties in the Skagit River Delta, northern Puget Sound, Washington—Juvenile Chinook salmon habitat availability in the Swinomish Channel, U.S. Geological Survey Scientific Investigations Report 2007-5120. U.S. Geological Survey, Reston, Virginia.
Hofmeister, R., Burchard, H., Bolding, K., 2009. A three-dimensional model study on processes of stratification and de-stratification in the Limfjord. Continental Shelf Research 29 (11–12), 1515–1524, http://dx.doi.org/10.1016/j.csr.2009.04.004.
Kim, B.O., 2003. Tidal modulation of storm waves on a macrotidal flat in the Yellow Sea. Estuarine, Coastal and Shelf Science 57 (3), 411–420, http://dx.doi.org/10.1016/S0272-7714(02)00369-4.
Kim, T.W., Cho, Y.K., 2011. Calculation of heat flux in a macrotidal flat using FVCOM. Journal of Geophysical Research 116 (C3), C03010, http://dx.doi.org/10.1029/2010JC006568.
Kim, T.W., Cho, Y.K., You, K.W., Jung, K.T., 2010. Effect of tidal flat on seawater temperature variation in the southwest coast of Korea. Journal of Geophysical Research 115 (C2), C02007, http://dx.doi.org/10.1029/2009JC005593.
Kirby, R., 2000. Practical implications of tidal flat shape. Continental Shelf Research 20 (10–11), 1061–1077.
Jay, D.A., Smith, J.D., 1990. Circulation, density distribution and neapspring transitions in the Columbia River estuary. Progress in Oceanography 25 (1–4), 81–112, http://dx.doi.org/10.1016/0079-6611(90)90004-L.
Lacy, J.R., Stacey, M.T., Burau, J.R., Monismith, S.G., 2003. Interaction of lateral baroclinic forcing and turbulence in an estuary. Journal of Geophysical Research 108 (C3), 3089, http://dx.doi.org/10.1029/2002JC001392.
Lee, H.J., Jo, H.R., Chu, Y.S., Bahk, K.S., 2004. Sediment transport on macrotidal flats in Garolim Bay, west coast of Korea: significance of wind waves and asymmetry of tidal currents. Continental Shelf Research 24 (7–8), 821–832, http://dx.doi.org/10.1016/j.csr.2004.01.005.
Marques, W.C., Fernandes, E.H.L., Moller, O.O., 2010. Straining and advection contributions to the mixing process of the Patos Lagoon coastal plume, Brazil. Journal of Geophysical Research 115 (C6), C06019, http://dx.doi.org/10.1029/2009JC005653.
Marques, W.C., Fernandes, E.H.L., Rocha, L.A.O., 2011. Straining and advection contributions to the mixing process in the Patos Lagoon estuary, Brazil. Journal of Geophysical Research 116 (C3), C03016, http://dx.doi.org/10.1029/2010JC006524.
Monismith, S., Burau, J.R., Stacey, M., 1996. In: Hollibaugh, J.T. (Ed.), Stratification dynamics and gravitational circulation in northern San Francisco Bay. San Francisco Bay: The Ecosystem. American Association for the Advancement of Science, San Francisco, Calif, pp. 123–153.
Munk, W.H., Anderson, E.R., 1948. Notes on a theory of the thermocline. Journal of Marine Research 7 (3), 276–295.
Nepf, H.M., Geyer, W.R., 1996. Intratidal variations in stratification and mixing in the Hudson estuary. Journal of Geophysical Research 101 (C5), 12079–12086.
Nicolle, A., Karpytchev, M., 2007. Evidence for spatially variable friction from tidal amplification and asymmetry in the Pertuis Breton (France). Continental Shelf Research 27 (18), 2346–2356, http://dx.doi.org/10.1016/j.csr.2007.06.005.
Pavel, V., 2012. Stratification on the Skagit River tidal flats. Ph.D. Dissertation. Woods Hole Oceanographic Institution/Massachusetts Institution of Technology Joint Program.
Peters, H., 1997. Observations of stratified turbulent mixing in an estuary: Neap-to-spring variations during high river flow. Estuarine, Coastal, and Shelf Science 45, 69–88, http://dx.doi.org/10.1006/ecss.1996.0180.
Peters, H., Bokhorst, R., 2001. Microstructure observations of turbulent mixing in a partially mixed estuary, Part II: salt flux and stress. Journal of Physical Oceanography 31, 1105–1119.
Rippeth, T.P., Fisher, N.R., Simpson, J.H., 2001. The cycle of turbulent dissipation in the presence of tidal straining. Journal of Physical Oceanography 31 (8), 2458–2471.
Ralston, D.K., Stacey, M.T., 2005a. Longitudinal dispersion and lateral circulation in the intertidal zone. Journal of Geophysical Research 110 (C7), C07015, http://dx.doi.org/10.1029/2005JC002888.
Ralston, D.K., Stacey, M.T., 2005b. Stratification and turbulence in subtidal channels through intertidal mudflats. Journal of Geophysical Research 110 (C8), C08009, http://dx.doi.org/10.1029/2004JC002650.
Ralston, D.K., Stacey, M.T., 2007. Tidal and meteorological forcing of sediment transport in tributary mudflat channels. Continental Shelf Research 27 (10–11), 1510–1527, http://dx.doi.org/10.1016/j.csr.2007.01.010.
Ralston, D.K., Geyer, W.R., Lerczak, J.A., Scully, M., 2010. Turbulent mixing in a strongly forced salt wedge estuary. Journal of Geophysical Research 115 (C12), C12024, http://dx.doi.org/10.1029/2009JC006061.
Ralston, D.K., Geyer, W.R., Traykovski, P.A., Nidzieko, N.J. Effects of estuarine and fluvial processes on sediment transport over deltaic tidal flats. Continental Shelf Research, in this issue.
Simpson, J.H., Bowers, D., 1981. Models of stratification and frontal movement in shelf seas. Deep-Sea Research 28 (7), 727–738.
Simpson, J.H., Brown, J., Matthews, J., Allen, G., 1990. Tidal straining, density currents, and stirring in the control of estuarine stratification. Estuaries 13 (2), 125–132.
Speer, P.E., Aubrey, D.G., 1985. A study of non-linear tidal propagation in shallow inlet estuarine systems Part 2: theory. Estuarine Coastal and Shelf Science 21 (2), 207–224.
Stacey, M.T., Ralston, D.K., 2005. The scaling and structure of the estuarine bottom boundary layer. Journal of Physical Oceanography 35 (1), 55–71.
Stacey, M.T., Monismith, S.G., Burau, J.R., 1999. Observations of turbulence in a partially stratified estuary. Journal of Physical Oceanography 29, 1950–1970.
Stacey, M.T., Burau, J.R., Monismith, S.G., 2001. Creation of residual flows in a partially stratified estuary. Journal of Geophysical Research 106 (C8), 17013–17,037, http://dx.doi.org/10.1029/2000JC000576.
Wang, B., Fringer, O.B., Giddings, S.N., Fong, D.A., 2009. High resolution simulations of a macrotidal estuary using SUNTANS. Ocean Modelling 26 (1–2), 60–85, http://dx.doi.org/10.1016/j.ocemod.2008.08.006.
Wang, B., Fringer, O.B., Gross, E.S., Giddings, S.N., Fong, D.A. Monismith, S.G. Modeling and understanding turbulent vertical mixing in a macrotidal salt wedge estuary. Journal of Geophysical Research. http://dx.doi.org/10.1029/2010JC006135, in press.
Webster, A.L., Ogston, A.S., Nittrouer, C.A. Delivery, reworking and export of fine-grained sediment across the sandy Skagit River tidal flats. Continental Shelf Research, submitted for publication.
Wiles, P.J., van Duren, L.A., Häse, C., Larsen, J., Simpson, J.H., 2006. Stratification and mixing in the Limfjorden in relation to mussel culture. Journal of Marine Systems 60 (1–2), 129–143, http://dx.doi.org/10.1016/j.jmarsys.2005.09.009.
Yang, Z.Q., Khangaonkar, T., 2009. Modeling tidal circulation and stratification in Skagit River estuary using an unstructured grid ocean model. Ocean Modelling 28 (1–3), 34–49, http://dx.doi.org/10.1016/j.ocemod.2008.07.004.

Please cite this article as: Pavel, V., et al., Processes controlling stratification on the northern Skagit Bay tidal flats. Continental Shelf Research (2012), http://dx.doi.org/10.1016/j.csr.2012.06.012